Stem Cell Reports
Article

OPEN ACCESS

Non-invasive Chamber-Specific Identification of Cardiomyocytes in Differentiating Pluripotent Stem Cells

Eva Brauchle,[1,2] Anne Knopf,[1,2,3] Hannah Bauer,[2] Nian Shen,[1,2] Sandra Linder,[1] Michael G. Monaghan,[1,2] Kornelia Ellwanger,[4] Shannon L. Layland,[1,2] Sara Y. Brucker,[2] Ali Nsair,[3,5] and Katja Schenke-Layland[1,2,3,5,*]

[1]Department of Cell and Tissue Engineering, Fraunhofer Institute for Interfacial Engineering and Biotechnology (IGB), Nobelstrasse 12, 70569 Stuttgart, Germany

[2]Department of Women's Health, Research Institute for Women's Health, Eberhard Karls University Tübingen, Silcherstrasse 7/1, 72076 Tübingen, Germany

[3]Department of Medicine/Cardiology, Cardiovascular Research Laboratories, David Geffen School of Medicine at UCLA, 675 Charles E. Young Drive South, MRL 3645, Los Angeles, CA 90095, USA

[4]Institute of Cell Biology and Immunology, University of Stuttgart, Allmandring 31, 70569 Stuttgart, Germany

[5]Co-senior author

*Correspondence: katja.schenke-layland@med.uni-tuebingen.de

http://dx.doi.org/10.1016/j.stemcr.2015.12.007

SUMMARY

One major obstacle to the application of stem cell-derived cardiomyocytes (CMs) for disease modeling and clinical therapies is the inability to identify the developmental stage of these cells without the need for genetic manipulation or utilization of exogenous markers. In this study, we demonstrate that Raman microspectroscopy can non-invasively identify embryonic stem cell (ESC)-derived chamber-specific CMs and monitor cell maturation. Using this marker-free approach, Raman peaks were identified for atrial and ventricular CMs, ESCs were successfully discriminated from their cardiac derivatives, a distinct phenotypic spectrum for ESC-derived CMs was confirmed, and unique spectral differences between fetal versus adult CMs were detected. The real-time identification and characterization of CMs, their progenitors, and subpopulations by Raman microspectroscopy strongly correlated to the phenotypical features of these cells. Due to its high molecular resolution, Raman microspectroscopy offers distinct analytical characterization for differentiating cardiovascular cell populations.

INTRODUCTION

The clinical use of cardiac cells derived from embryonic and induced pluripotent stem cells (ESCs and iPSCs) is a promising and potentially patient-tailorable approach to address myocardial disease. ESCs and iPSCs have an unlimited capacity to self-renew and derive cardiovascular cells (Burridge et al., 2012; Zwi et al., 2009). However, guiding pluripotent stem cell differentiation into defined cardiac cell populations is still a major challenge. In contrast to undifferentiated ESCs that form tumors in vivo (Amariglio et al., 2009), cells directed toward the cardiac lineage in vitro can integrate and support heart function when delivered in vivo (Leor et al., 2007; Nsair et al., 2012). Culture protocols for deriving heterogeneous cell populations that resemble the fetal developmental stages of atrial and ventricular cardiomyocytes (CMs) from pluripotent stem cell sources use versatile biological, chemical, and/or physical factors, and to identify the cardiac differentiation states requires laborious analytical procedures based on intracellular markers (Mummery et al., 2012; Schenke-Layland et al., 2008). Patient-specific iPSC-derived CMs offer a new paradigm for disease-modeling-in-a-dish, as well as drug screening and discovery (Matsa et al., 2014); however, it will be imperative to monitor chamber specificity and maturity of the pluripotent cell-derived CMs in real time and preferably marker free. To date, the methods of choice to determine the developmental stage of differentiating pluripotent stem cell-derived CMs include invasive gene and protein expression profiling of harvested cells, or electrophysiological analyses via patch clamp technologies (Karakikes et al., 2014). Cardiac promoters were used to drive expression of the fluorescent reporter gene EGFP to allow identification and sorting of atrial- or ventricular-like CMs differentiated from pluripotent cell sources (Huber et al., 2007). However, such genetic manipulation for the purpose of cell purification is rather laborious, and most of all, it limits the clinical usability of the cells.

Raman microspectroscopy is a marker-free method that can be used to characterize single cells based on a pattern of molecular vibrational modes, which reflects the composition of intracellular proteins, lipids, nucleic acids, and carbohydrates (Puppels et al., 1990). Notingher et al. (2004) investigated changes in Raman spectra due to cellular differentiation and demonstrated that the method, in combination with principal component analysis (PCA), can be used as a tool for discriminating pluripotent cells from their cardiac progeny (Pascut et al., 2011). Our group has integrated a custom-made Raman spectroscopic system with a fluorescence microscope to demonstrate that Raman

signal patterns can be correlated to specific cell phenotypes and stages (Brauchle et al., 2014). Here, we employed Raman microspectroscopy to acquire biochemical fingerprints of the right atrium (RA), right ventricle (RV), left atrium (LA), and left ventricle (LV) of murine and human heart tissues. We further assessed biochemical shifts specific for cardiovascular lineage commitment and cardiac specification in differentiating murine and human ESCs (mESCs and hESCs) employing PCA on the spectral data (Figure S1). The unique combination of Raman spectroscopy with high-resolution fluorescence microscopy allowed the collection of Raman profiles of mESC- and hESC-derived CMs with an atrial or ventricular specification. Raman patterns and spectral differences were verified by analyzing fetal murine (mfCMs) and human CMs (hfCMs). We further identified that alterations of cardiac protein expression patterns, which occur after birth when CMs adapt to their specific physiological tasks (Sylva et al., 2014), also correlate to specific shifts in the cardiac Raman signature and thus Raman microspectroscopy was used to assess the maturity of the in vitro-generated ESC-derived CMs.

RESULTS

Heart Tissue Exhibits Atria- and Ventricle-Specific Raman Profiles

The difference in the thickness of the atrial and ventricular myocardium is a well-described histoanatomical feature, which reflects the amount of force each chamber is required to generate in order to pump the blood out of the adult heart (Figure 1Aa). Although both atria are much thinner than the ventricles, expression of contractile proteins such as sarcomeric myosin (MF20) and cardiac troponin (cTNT) is found equally in the CMs of all heart chambers (Figures 1Ab and 1Ac). Raman microspectroscopy was employed to explore molecular patterns in the different anatomical sites of the myocardium (LA, RA, RV, and LV) utilizing formalin-fixed paraffin-embedded (FFPE) hearts of adult (8 months old) mice. Although we identified that FFPE processing may impact lipid Raman signals (Figure S2A), our data showed that the Raman spectra specific for LA and RA, as well as RV and LV, were predominantly assignable to signals from proteins (Figure 1Ad and Table 1), which were unaltered due to tissue processing. By employing PCA, spectral differences that determine the separation of atria and ventricles were depicted in principal component 2 (PC 2) (Figures 1Ae and S2B). The further analysis of PC 2 loadings confirmed that Raman signals at 938, 1003, 1342 cm^{-1} and the amide I signal at 1658 cm^{-1} were indeed stronger in the atria compared to the ventricles (Figure 1Ad), indicating a highly distinct protein content and structure in the atrial versus the ventricular myocardium (Table 1).

Both atria and ventricles septate during early development and adapt their specific physiological function (Sylva et al., 2014). To investigate if the identified spectral differences may be impacted by the developmental stages, we recorded chamber-specific Raman profiles in murine fetal hearts at stage E15.5. Anatomically, fetal hearts exhibit rather large atria and two morphologically similar ventricles, where the compact myocardium of the LV is slightly thicker than that of the RV (Figure 1Ba). Immunofluorescence staining confirmed the expression and alignment of sarcomeric proteins in both atria (Figure 1Bb) and ventricles (Figure 1Bc) at this stage. In contrast to the Raman spectra obtained from adult hearts, the signals that were collected from fetal murine heart tissues were noisier and more heterogeneous in their peak patterns (Figure 1Bd). Due to these spectral characteristics, significant differences between murine fetal atria and ventricles were described in higher PCs. The most significant differences were identified in scores of PC 5 and PC 7 (Table S1). By plotting the score values of PC 5 and PC 7, Raman spectra separated in two clusters: one cluster included the spectra from both atria and a second cluster was formed by the spectra from LV and RV (Figure 1Be). Based on the PC 7 loading, the Raman peaks at 1003 and 1342 cm^{-1}, which represent structural protein shifts (Table 1), were identified to have a high impact on the differentiation between murine fetal atria and ventricles (Figures 1Bd and S2C).

In human hearts from the corresponding developmental stage of 8–10 weeks after gestation (Sylva et al., 2014), a strong LV, much thicker than the RV, was observed (Figure 2A). As expected, LA and RA were much smaller compared to the ventricles (Figure 2A). Although myofibrillar proteins were present and aligned in the atria and ventricles (Figures 2B and 2C), Raman spectra of LA, RA, RV, and LV from human fetal FFPE heart tissues showed a high amount of spectral noise and strong spectral variations when comparing the different heart chambers (Figure 2D), similar to what was observed in the mouse tissues. PCA helped to reduce the spectral noise, and score values supported the identification of significant differences in the spectra of FFPE heart tissues. Molecular information specific for either atria or ventricles was identified in PC 5 (Table S1). Separate clusters for human fetal atrial and ventricular tissues were identified when plotting PC 5 score values (Figure 2E). The PC 5 loading indicated a high impact of the Raman peaks at 1003, 1358, 1387, 1426, 1486 cm^{-1} on this separation (Figure S2C). These molecular differences between human fetal atria and ventricles can be attributed to vibrational modes of proteins (Table 1).

Overall, the multivariate analysis of Raman signals from FFPE heart tissues revealed molecular differences in the

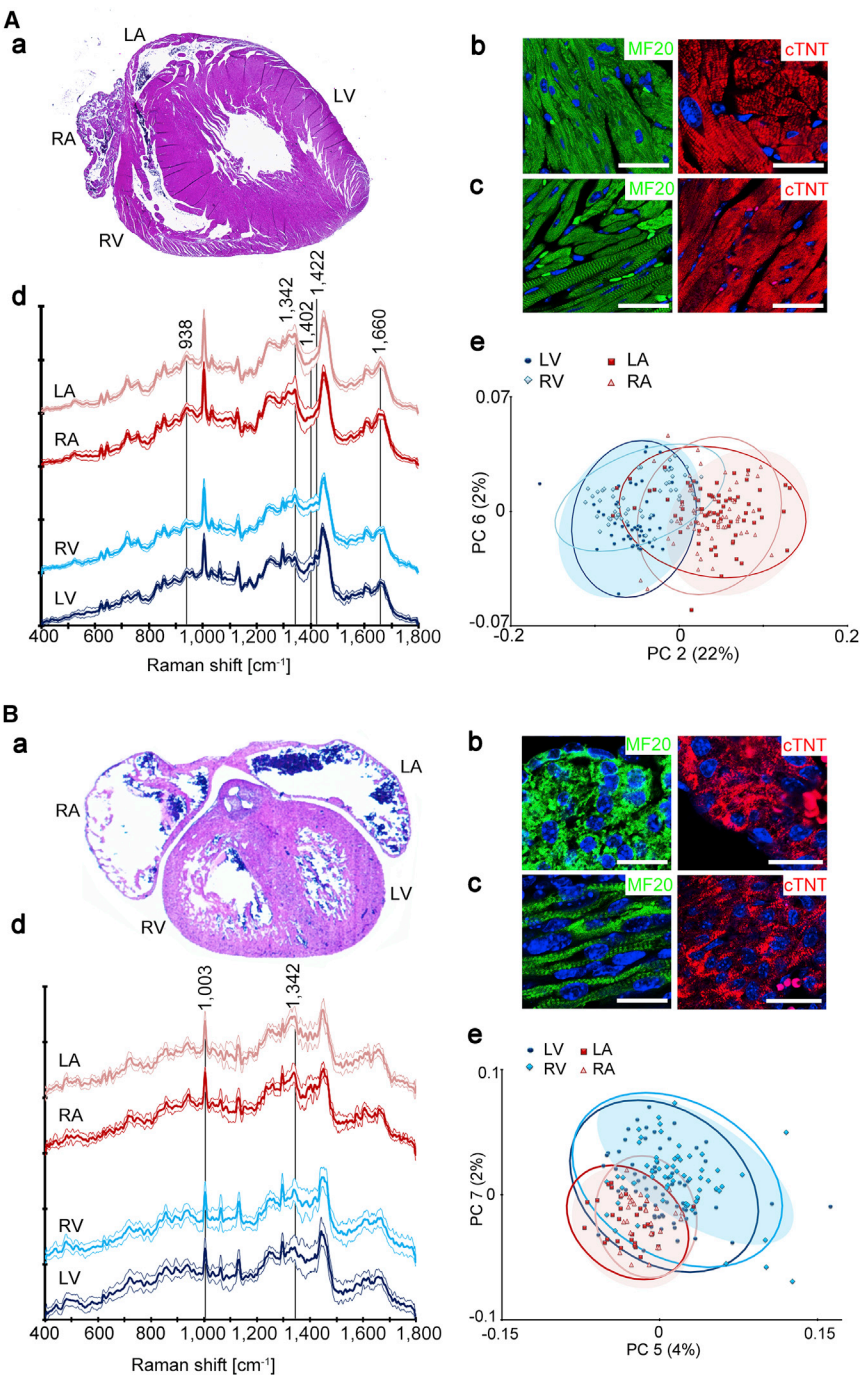

Figure 1. Identification of Atrial and Ventricular Raman Signatures in Sections of Murine Adult and Fetal Hearts

H&E staining of an (Aa) adult and (Ba) fetal heart displays the four chambers (LA, left atrium; LV, left ventricle; RA, right atrium; RV, right ventricle). MF20 (green) and cTNT (red) are expressed in (Ab, Bb) atria and (Ac, Bc) ventricles. Nuclei are stained with DAPI (blue). Scale bars equal 20 μm. (d) Raman spectra acquired from the LA, RA, RV, and LV in (Ad) adult and (Bd) fetal heart tissues. Both adult and fetal atria show significantly higher relative intensities at the Raman shift 1342 cm^{-1}. (e) Multivariate analysis of the Raman spectra depicts the differences between atria and ventricles via (Ae) PC 2 in adult hearts, respectively (Be) PC 7 in fetal hearts. See also Figures S2B, S2C, and S3.

atria and ventricles (Figures 1Ac, 1Bc, 2C, and S2C). In mouse and human hearts, the Raman spectra showed a clear separation of atria and ventricles due to structural protein modes. To further investigate if these Raman signals arose from the CMs in the right and left atria and ventricles, we explored Raman profiles obtained from primary isolated CMs from murine adult atria and ventricles. Based on PCA, it was corroborated that spectral differences assigned to protein conformational modes allow for the discrimination of both atrial and ventricular CMs at the single-cell level (Figures S3A and S3B). However, besides CMs, cardiac fibroblasts are an abundant cell population in the fetal and adult heart (Sylva et al., 2014). Since fibroblasts represent a common contaminant when isolating CMs from primary tissues or stem cell cultures, it is of high interest to distinguish between CMs and fibroblasts in a label-free manner

Table 1. Annotations of Raman Peaks Identified in Chamber Specificity and Cardiac Fate Commitment

Raman Shift (cm^{-1})	Assignment	References
486	glycogen	Pascut et al., 2011; Chan et al., 2009
701	cholesterol	Krafft et al., 2005
770–830	nucleic acids	Puppels et al., 1990; Tan et al., 2012
938	proteins in alpha-helix conformation, troponin T, myosin, tropomyosin	Pascut et al., 2011; Pézolet et al., 1988
988	proteins in beta-sheet conformation	Pézolet et al., 1988
1003	phenylalanine	Puppels et al., 1990
1065	cholesterol	Krafft et al., 2005
1095	phosphate backbone of nucleic acids	Tan et al., 2012; Pézolet et al., 1988
1230–1360	amide III, troponin T, myosin, tropomyosin	Pascut et al., 2011; Pézolet et al., 1988
1380–1490	CH, CH_2, CH_3 vibrations NH in plane vibrations	Krafft et al., 2005; Pézolet et al., 1988
1640–1680	amide I, troponin T, myosin	Pascut et al., 2011; Pézolet et al., 1988

(Nunes et al., 2013; Sylva et al., 2014). In contrast to cardiac fibroblasts, CMs express sarcomeric proteins, which contribute to the unique spectral CM fingerprint (Figures S3C, S3E, and Table 1). Moreover, PCA showed a clear distinction between cardiac fibroblasts and CMs based on the spectral patterns, and therefore encourages the possibility of spectra-based identification and separation of murine and human CMs (Figures S3D and S3F).

Raman Microspectroscopy as a Tool for Marker-free Monitoring of Pluripotent Stem Cell Differentiation toward the Cardiac Cell Lineage

To monitor cardiac cell fate commitment, mESCs and hESCs were differentiated toward the cardiac cell lineage following established protocols (Kattman et al., 2011; Schenke-Layland et al., 2008). According to these previous reports (Kattman et al., 2011; Schenke-Layland et al., 2008), embryoid body (EB) formation and induction of differentiation resulted in downregulation of pluripotency genes and upregulation of the expression of lineage-specific proteins (Figures 3A and S4A). FLK1-expressing precardiac mesoderm was observed in murine EB cultures after 6 days of differentiation (Figure 3A). At this stage, murine cardiovascular progenitor cells (CPCs) were isolated and purified using magnetic bead sorting prior to the Raman measurements (Figure S4B). The expression of cTNT after 10 more days in culture indicated progression of cardiac differentiation (Figure 3A). Spontaneously beating mESC-CMs were harvested from murine EB cultures after 18–21 days of differentiation, which were then immediately exposed to Raman spectroscopic analyses in suspension (Video S1). Raman spectra clearly identified different molecular profiles for mESCs, mCPCs, and mESC-CMs (Figure S4C). PC scores of spectra from single cells were subjected to statistical analyses (Table S2). By plotting PC 3 versus PC 7 scores, a transition from mESCs to mCPCs and mESC-CMs was evident (Figure 3B). When analyzing the PC 3 loading, Raman shifts at 701, 784, 1065, 1320, and 1437 cm^{-1} were determined to indicate cardiac commitment and differentiation (Figure 3C). To investigate if these Raman signatures could be used in a predictive manner for the identification of cardiac cells within heterogeneous cultures, a PCA-linear discriminant analysis (LDA) was employed on the datasets (Chan et al., 2009). When applying testing data on this PCA-LDA model, 95% of the spectra from mESCs were categorized as such; the sensitivity for discriminating mCPCs and mCMs was 44% (Table S3). These results were consistent with the plot of the PCA scores, where the clusters of mCPCs and mESC-CMs overlapped (Figure 3B).

In cultures of human EBs, stage-specific growth factors guided cardiac differentiation, which was evident after 10 days of differentiation, when spontaneous beating of EBs was observed (Video S2). Moreover, at this time point, the expression of cTNT, MF20, and CX43 confirmed cardiac differentiation (Figures 3D and S5A). In terms of cell morphology and cTNT expression patterns, hESC-CMs were highly comparable with hfCMs (Figure 3D and Video S3). When subjecting the Raman spectra acquired for single hESCs, hESC-CMs, and hfCMs to PCA, most significant differences were observed between hESCs and hfCMs in PC 1, which were assignable to glycogen (Figure S5B and Table 1). Similarities of hESC-CMs and hfCMs were evident in PC 4 score values (Table S2). Plotting PC 1 versus PC 4 scores separated the spectra of hESCs from hfCMs and indicated successive spectral shifts due to the progression of cardiac differentiation (Figure 3E). We identified wavenumbers 486, 701, 784, 1003, 1065, 1320, and 1437 cm^{-1} as predominantly affected during human cardiac differentiation (Figure 3F). These signals suggest a decrease in nucleic acids and an increase of lipids and cholesterol due to cardiac differentiation (Table 1). Most interestingly, many analogous Raman peaks were identified in the analysis of Raman spectra from murine cells (Figures 3C and 3F), which suggests that these cellular components might have a species-independent key role in cardiac cell fate commitment and differentiation. Moreover, our results demonstrate that

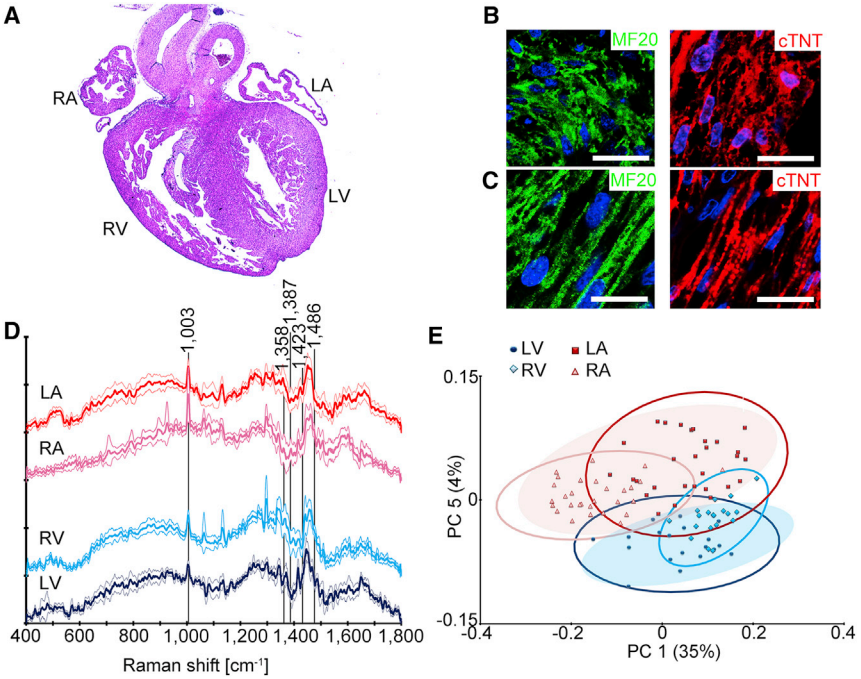

Figure 2. Molecular Differences in Atria and Ventricles of the Human Fetal Heart

(A–C) H&E staining displays the four heart chambers in the human fetal heart (A). LA, left atrium; LV, left ventricle; RA, right atrium; RV, right ventricle. Immunofluorescence staining (MF20, green; cTNT, red) of the (B) atria and (C) ventricles. DAPI (blue) shows cell nuclei. Scale bars represent 20 μm.

(D) Raman spectra collected from LA, RA, RV, LV detected in human fetal heart sections. Differences between atria and ventricles were identified at the wavenumbers 1003, 1358, 1387, 1423, 1486 cm^{-1}.

(E) PCA depicting distinct populations for spectra collected from atria (red) and ventricles (blue). See also Figures S2D and S3.

Raman spectra and PCA are potentially capable of supporting marker-free identification of stem cell-derived cardiac cells within heterogeneous cultures.

Raman Profiles Identify Chamber-Specific Murine and Human ESC-CMs

The commitment of CMs to atrial or ventricular phenotypes occurs early in development during linear heart tube formation and can also be observed in stem cell-derived CMs (Mummery et al., 2012). Based on the expression of myosin light chain 2 (MLC2) isoforms, atrial and ventricular CMs can be distinguished (Mummery et al., 2012). This distinction of atrial and ventricular CMs is important when stem cell-derived cells are to be considered for disease modeling, drug screening and discovery, and for clinical regenerative therapies. High-resolution fluorescence imaging was performed simultaneously to Raman spectra acquisition to investigate whether Raman microspectroscopy can identify atrial and ventricular CM phenotypes derived from pluripotent stem cells (Brauchle et al., 2014). For this purpose, all murine and human cells were fixed and stained for MLC2a (atrial isoform of MLC2) and MLC2v (ventricular isoform of MLC2). In addition to ESC-CMs, we processed fetal CMs in the same fashion for verification of the Raman patterns from $MLC2a^+$ and $MLC2v^+$ CMs (Figures 4 and 5).

Although both mfCMs and mESC-CMs maintained MLC2a or MLC2v expression after cell isolation and attachment, the structural organization of both proteins lacked distinctive striated myofibrillar patterns (Figures 4A, 4B, 4E, 4F, and S4D). Raman spectra were collected from freshly isolated and antibody-labeled $MLC2a^+$ and $MLC2v^+$ mfCMs and mESC-CMs in suspension (Figures 4C and 4G). Plotting of the PC scores of the Raman spectra from $MLC2a^+$ and $MLC2v^+$ mfCMs revealed two clearly separated populations (Figure 4D and Table S4). The PC 3 loading highlighted the wavenumbers 1265, 1336, 1386, 1660 cm^{-1} as having a great influence on this separation of atrial and ventricular mfCMs (Figure S2E). Our data showed that $MLC2a^+$ mfCMs exhibited stronger signals in 1265 and 1660 cm^{-1}, whereas in Raman spectra from $MLC2v^+$ mfCMs, signals at 1336 and 1386 cm^{-1} were more pronounced (Figure 4C). PCA of the vibrational signals of single $MLC2a^+$ and $MLC2v^+$ mESC-CMs also showed two distinct populations (Figure 4H). The spectral shifts that indicate atrial and ventricular commitment emerged in PC 3 and PC 4 (Figure 4H and Table S4). Based on the PC 4 loading pattern, the Raman peaks at 1336 and 1670 cm^{-1} were identified to have a strong impact on spectra of $MLC2a^+$ mESC-CMs, whereas the influence of vibrational signals at Raman shifts 1408 and 1437 cm^{-1} was more pronounced in $MLC2v^+$ mESC-CMs. Furthermore, the Raman signals at 786 and 1095 cm^{-1} had an effect on the PCA-based distinction of $MLC2a^+$ versus $MLC2v^+$ mESC-CMs and were more prominent in the spectra of $MLC2a^+$ mESC-CMs (Figures 4G and S2G).

Our results showed that mouse atrial CMs differ from ventricular CMs in the amide I peak, which is indicative for protein conformational modes in $MLC2a^+$ mfCMs compared to $MLC2v^+$ mfCMs (Table 1). In hfCMs, isolated

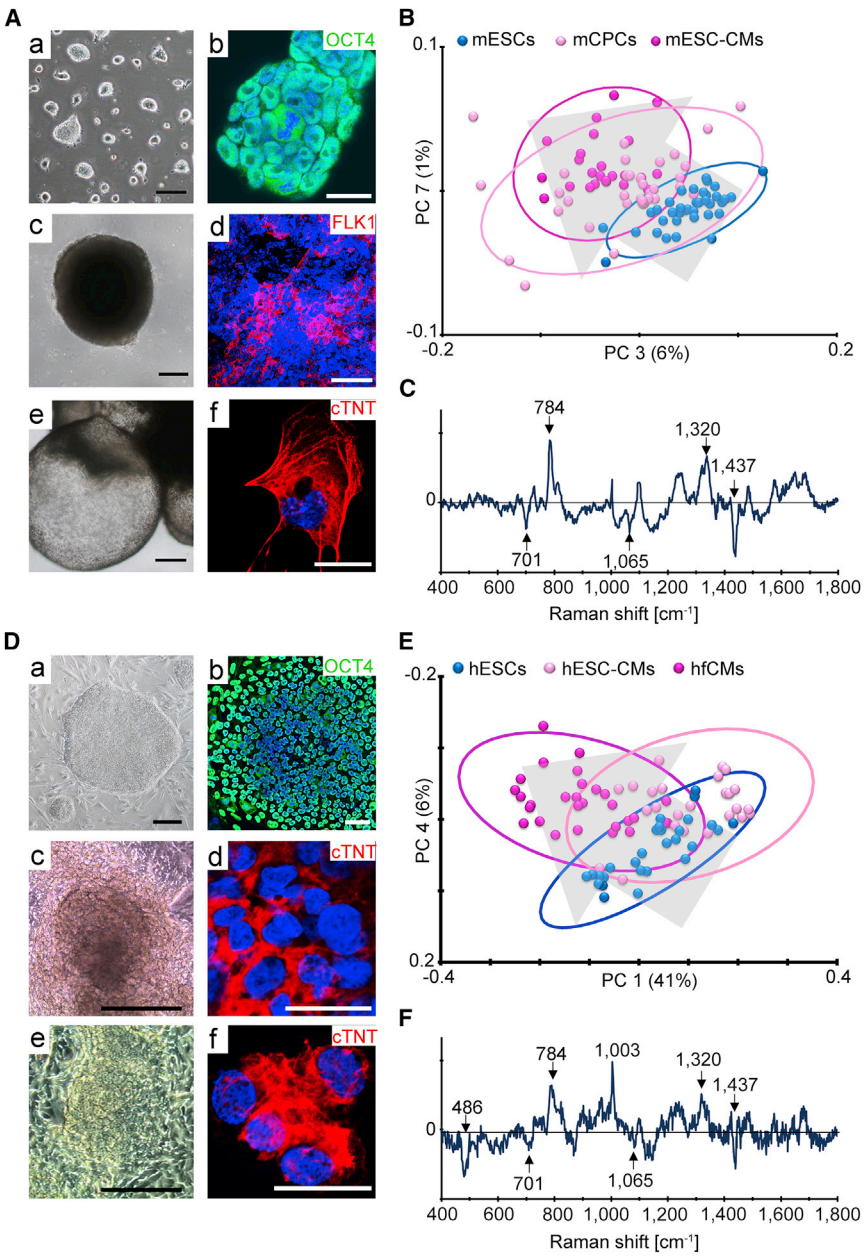

Figure 3. Differentiation of Mouse and Human Embryonic Stem Cells Toward Cardiomyocytes Monitored by Immunofluorescence Staining and Raman Microspectroscopy

(A) Bright field (a, c, e) and immunofluorescence microscopy (b, d, f) of mESCs and embryoid bodies containing cardiovascular progenitor cells (CPCs) (c, d), and cardiac troponin T (cTNT)-positive mESC-derived cardiomyocytes (ESC-CMs). Scale bars equal 200 μm (a, c, e) and 50 μm (b, d, e).

(B) Scores of principal component (PC) 3 and PC 7 for Raman spectra of mESCs, mCPCs, and mESC-CMs. The arrow indicates cardiac differentiation.

(C) PC 3 loading presents the Raman peaks that change significantly due to cardiac commitment and differentiation.

(D) Morphology of (a) hESC colonies, (c) hESC-CMs, and (e) human fetal CMs (hfCMs). Scale bars equal 200 μm. Fluorescence microscopy of Oct4 staining on (b) hESCs and cTNT staining of (d) hESC-CMs and (f) fhCMs. Scale bars represent 20 μm.

(E) Scores of PC 1 and PC 4 of Raman spectra from hESCs, hESC-CMs, and hfCMs demonstrate successive spectral changes due to cardiac differentiation highlighted by the arrow.

(F) Raman peaks with successive change from hESCs to hESC-CMs and hfCMs are illustrated by loading of PC 4. Peaks that are consistent with the murine pattern in (C) are indicated. See also Figures S4 and S5.

from 8- to 9-week-old hearts, the expression of MLC2a and MLC2v was determined after cell isolation and attachment (Figures 5A and 5B). Raman spectra specifically generated from MLC2a$^+$ and MLC2v$^+$ hfCMs exhibited a high SD resembling the high heterogeneity of these cell populations (Figure 5C). When analyzing these spectra with PCA, significant differences ($p < 0.05$) between MLC2a$^+$ and MLC2v$^+$ hfCMs were identified in the PC 3 scores (Table S4). The PC scores plot, including PC 2 and PC 4, depicted two cell populations for MLC2a$^+$ and MLC2v$^+$ hfCMs but also an intermediate zone where both populations overlapped (Figure 5D). For the spectral distinction of MLC2a$^+$ and MLC2v$^+$ hfCMs, the wavenumbers 1096, 1320, 1336, 1375, and 1423 cm^{-1} had a high impact on the separation of MLC2a$^+$ and MLC2v$^+$ hfCMs (Figure 5C and S2F). Interestingly, MLC2a expression in hESC-CMs showed an organized myofibrillar structure and alignment (Figure 5E), whereas MLC2v expression was rather low and was detected in significantly fewer cells compared with MLC2a$^+$ hESC-CMs (Figures 5F and S5C). Despite these differences in protein expression, Raman spectra acquired from MLC2a$^+$ and MLC2v$^+$ hESC-CMs showed congruence with lower SDs compared to the primary isolated fetal cells (Figure 5G). In depth PCA revealed

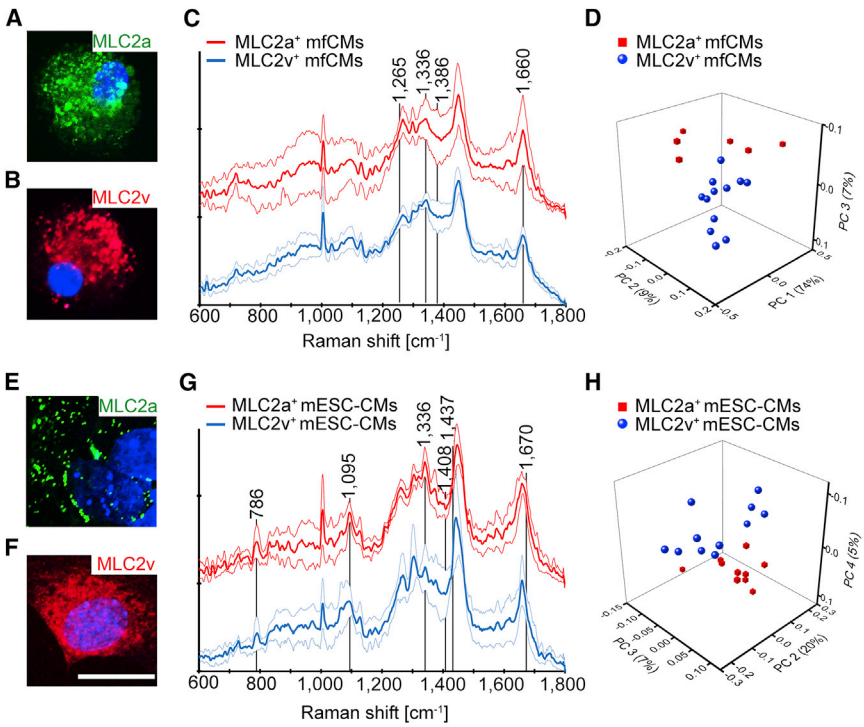

Figure 4. Identification of Atrial and Ventricular Specification in Murine Fetal Cardiomyocytes and Murine Embryonic Stem Cell-Derived Cardiomyocytes

(A and B) Fluorescence microscopy of mfCMs isolated from the atria and stained for (A) MLC2a and (B) mfCMs that were isolated from the ventricles identified by MLC2v expression.

(C) Based on MLC2a and MLC2v expression, atrial and ventricular mfCMs were identified and Raman microspectroscopy was performed on the single antibody-labeled cells. Vertical lines highlight wavenumbers identified in the principal components (PCs).

(D) Scores plot of the spectra depicts differentiation of MLC2a$^+$ and MLC2v$^+$ mfCMs via PC 1, 2, and 3. mESC-CMs stained for (E) MLC2a and (F) MLC2v to detect atrial and ventricular specification. Scale bar represents 20 μm.

(G) Raman spectra recorded from MLC2a$^+$ and MLC2v$^+$ mESC-CMs, highlighting the wavenumbers of the most prominent differences.

(H) PC scores plot visualizes two clusters based on the spectra. See also Figures S2E and S2G.

significant differences in Raman spectra in PC 3 and PC 4 scores from MLC2a$^+$ and MLC2v$^+$ hESC-CMs (Figure 5H and Table S4). Two separated hESC-CM populations were visualized in the PCA scores plot, although few MLC2a$^+$ hESC-CMs clustered with MLC2v$^+$ hESC-CMs and vice versa (Figure 5H). The closer investigation of the PC 4 loading pattern elucidated a stronger influence of the Raman peaks at 788, 1336, 1362, and 1380 cm^{-1} on the spectra from MLC2v$^+$ hESC-CMs compared with those from MLC2a$^+$ hESC-CMs (Figure S2H). Furthermore, PC 4 depicted a shift in the spectra of MLC2v$^+$ hESC-CMs in the amide I region around 1658 cm^{-1} (Figures 5G and S2H). Similar to the PCA-based separation of hfCMs, we identified overlaps between the clusters of MLC2a$^+$ hESC-CMs with those of MLC2v$^+$ hESC-CMs (Figure 5H). Additional immunofluorescence staining of human fetal heart tissues visualized ventricular CMs co-expressing both proteins (Figure S5D). The presence of double-positive MLC2a$^+$/MLC2v$^+$ CMs might explain the overlap of both CM subtypes in the PCA scores plot (Figure 5D), where both MLC2a or MLC2v expression was considered in single cells.

Raman Microspectroscopy Allows the Label-free Monitoring of Cardiac Maturation

For in vitro drug screening, CMs must exhibit a mature fully functional cardiac phenotype in order to mimic normal cardiac physiology (Matsa et al., 2014). However, CMs derived from pluripotent stem cell sources using standard differentiation protocols resemble an immature fetal phenotype (Matsa et al., 2014). As expected when using standard cardiac in vitro differentiation protocols, in our study, mESC-CMs showed incomplete alignment and insufficient sarcomeric myosin striation (Figure 6Ab). In vivo, CMs undergo substantial metabolic and structural evolution after birth (Pasumarthi and Field, 2002; Siedner et al., 2003), resulting in morphological changes as well as an increase in the expression level of myofibrillar proteins (Figure 6Af). In correlation with these known features, Raman spectra of mESC-CMs and mfCMs showed clear differences compared with the spectra of murine adult CMs (Figure S6A). PCA confirmed this result and further revealed that the significant differences were identified in the PC 3 and PC 4 score values (Figure 6B and Table S5). The PC 3 loading spectrum highlights that Raman signals at 1266, 1437, and 1658 cm^{-1}, which indicate proteins and lipids, increased due to the postnatal maturation of CMs (Figure 6C and Table 1). Nucleic acid-specific modes at 787 and 1095 cm^{-1} decreased, and were more pronounced in mESC-CMs and mfCMs (Table 1). Interestingly, these differences in the Raman spectra were also observed in fetal versus adult FFPE tissues (Figures S6B and S6C).

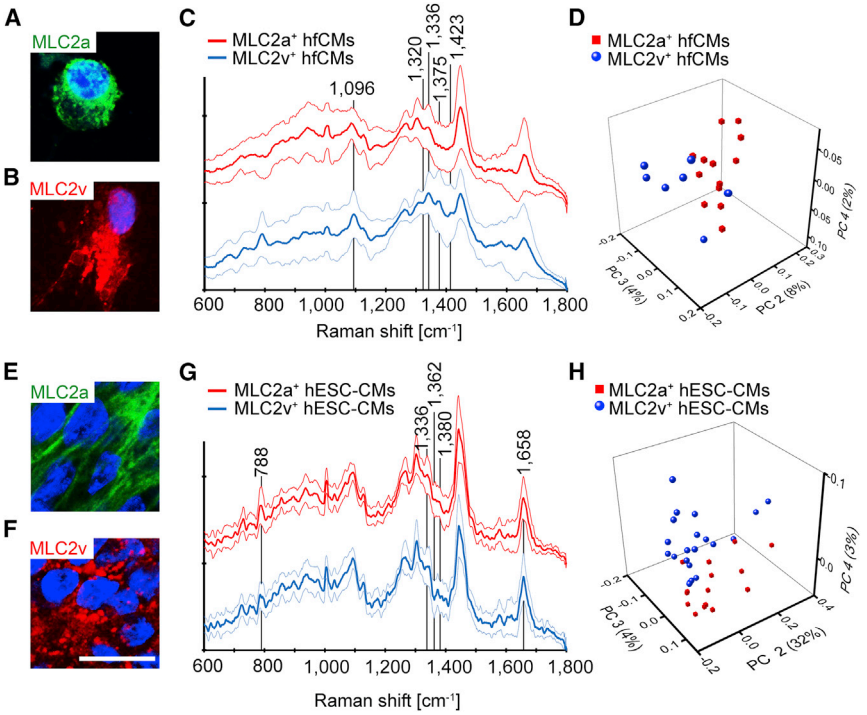

Figure 5. Characterization of Atrial and Ventricular Phenotypes in Human Fetal Cardiomyocytes and Human Embryonic Stem Cell-Derived Cardiomyocytes

(A and B) Detection of atrial and ventricular fhCMs via (A) MLC2a and (B) MLC2v staining. Scale bar equals 20 μm.

(C and D) Raman spectra and data analysis of MLC2a$^+$ and MLC2v$^+$ fhCMs.

(D) Scores plot of the spectra depicts differentiation of MLC2a$^+$ and MLC2v$^+$ mfCMs via PC 2, 3, and 4. Atrial and ventricular specification of hESC-CMs detected by (E) MLC2a and (F) MLC2v expression.

(G) Raman microspectroscopy of MLC2a$^+$ and MLC2v$^+$ hESC-CMs.

(H) PC scores plot visualizes a distinction between MLC2a$^+$ and MLC2v$^+$ CMs based on Raman data. See also Figures S2D and S2F.

DISCUSSION

This study demonstrates the power of Raman microspectroscopy as an optical marker-free technology to assess cardiovascular commitment, cardiac differentiation, and cardiac maturation in primary isolated cells and tissues, as well as cells and tissue equivalents (EBs) derived from pluripotent stem cell sources. Species-independent changes due to cardiovascular cell fate commitment and differentiation were identified based on Raman profiles acquired from murine and human cells. Phenotype-specific cardiac signals, which can be used to differentiate between atrial and ventricular CMs that are derived from pluripotent stem cells, were identified using multivariate analysis. Moreover, we showed that Raman microspectroscopy is a suitable tool to assess cardiac maturity in living single CMs as well as cardiac tissues. To date, no other modality has non-invasively demonstrated such clear specification of stem cell-differentiated CMs based on chamber and developmental stage.

Nevertheless, technological improvements and adaptions will be necessary to achieve the transition of Raman microspectroscopy from a tool for research and development purposes to a routine device for the marker-free single-cell sorting and high-throughput analysis. In a very elegant study, Dochow et al. (2013) showed the feasibility of Raman spectroscopy and cell sorting in a microfluidic chamber. The further reduction of measurement times and the establishment of automated software to facilitate spectral analysis, and for non-experienced users, are currently addressed by other groups (Ren et al., 2014; Richardson et al., 2014).

Our microspectroscopic approach shows that mESCs, hESCs, and their cardiac progeny exhibit unique molecular fingerprints, and the acquisition of Raman spectral data from such biological materials provides insights into molecular and developmental cell biology processes, potentially enabling the identification of molecular drivers in cell differentiation pathways (Sule-Suso et al., 2014). The Raman spectra obtained from ESCs were consistent with data published by others (Chan et al., 2009). As previously described, mESC molecular fingerprint patterns showed characteristic signals that can be attributed to nucleic acids (Notingher et al., 2004). Here, we detected only median nucleic acid peaks, but stronger signals from lipids at 1300, 1437, and 1658 cm^{-1} (Krafft et al., 2005) in hESCs. Culture conditions as well as cell line-specific variations, which are controversially discussed for pluripotent stem cells (Burridge et al., 2012), could impact the molecular Raman signature. Tan et al. (2012) showed that differences in the spectra of hESCs and hiPSCs are only minimal compared with the spectral shifts that occur due to cell differentiation. This is consistent with our data presented in this study, where cardiac differentiation led to specific molecular changes in the cellular fingerprint spectrum of pluripotent cells. Namely, cardiac cell fate commitment was detectable by an increase of the Raman bands at 701, 1065, and 1437 cm^{-1} in human and murine cells. These

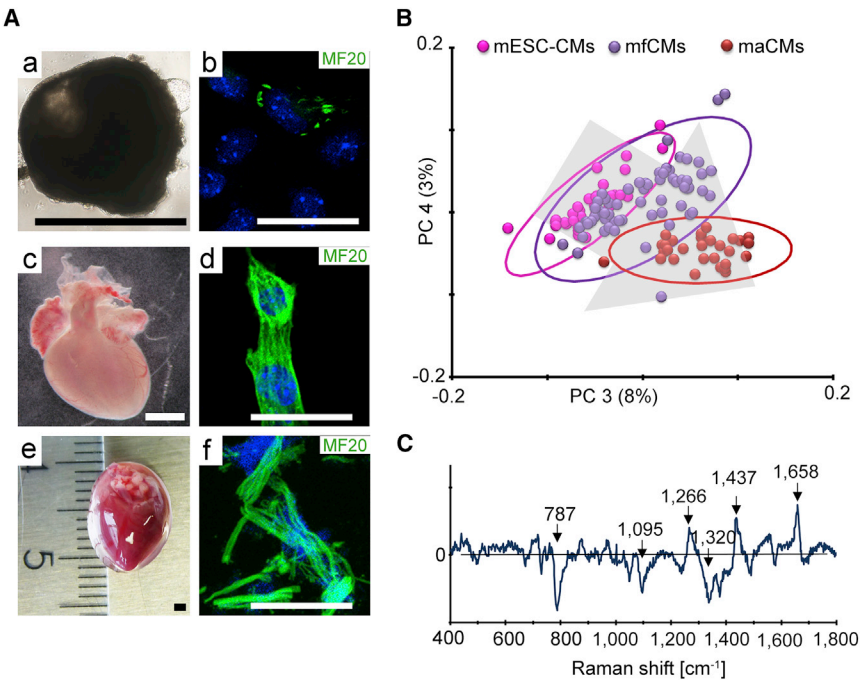

Figure 6. Comparison of Murine Embryonic Stem Cell-Derived CMs, Murine Fetal CMs, and Murine Adult CMs

(A) mESC-derived EB (a), fetal (c), and adult hearts (e) before cell isolation, and sarcomeric myosin (MF20, green) expression patterns in mESC-CMs (b), mfCMs (d), and maCMs (f). Scale bars represent 1 mm (a, c, e) and 20 μm (b, d, f).

(B) Plot of PC 3 and PC 4 score values derived from Raman spectra of mESC-CMs, mfCMs, and maCMs indicate maturation from a fetal to an adult CM phenotype (indicated by the direction of the gray arrow).

(C) PC 3 loading describes the Raman shifts that vary in mature maCMs compared to mESC-CMs and mfCMs. See also Figure S6.

Raman bands can be assigned to cholesterol but also other lipid molecules (Krafft et al., 2005). Although it has been described that lipids play a role in energy storage and homeostasis in cardiac muscle, the role of lipid metabolism and energy storage in cardiac cell fate decisions has not been fully understood. The metabolic machinery of ESCs, in contrast to ESC-CMs, is reported to be only rudimentarily developed (Chung et al., 2007). In cardiac differentiation, successive remodeling of this metabolic system has been identified to orchestrate the alignment of mitochondria and cardiac-specific key regulators for high energy-dependent CMs (Chung et al., 2007). Cholesterol-rich membrane domains, cholesterol signaling, and lipid metabolism might play a role in early cardiac cell fate decisions as the Raman profiles of ESCs, CPCs, and ESC-CMs vary significantly. To our knowledge, this is the first report in which Raman microspectroscopy was employed for CPC characterization. To further elucidate CPC subpopulations, the spectroscopic data could be correlated with data of cellular metabolism and protein expression to subspeciate this heterogeneous population.

ESC-CMs can be subdivided into atrial and ventricular CMs (Burridge et al., 2012). It has been documented that the expression of the α-isoform of myosin heavy chain (α-MHC), MLC2a, and MLC1a become restricted to the atrium during murine development (Zammit et al., 2000). Here, we employed MLC2a and MLC2v immunocytological staining to identify murine and human CM subtypes and demonstrated that Raman microspectroscopy can identify atrial and ventricular CM subpopulations derived from pluripotent murine and human cells. Atrial and ventricular CMs exhibit differences in the expression and organization of structural proteins (Bird et al., 2003; Zammit et al., 2000). We identified structural protein signals (938, 1265, 1658 cm^{-1}) as highly relevant for the spectral-based differentiation of atrial and ventricular CMs. Muscle fibers, including myosin proteins, contain predominantly alpha-helical conformations, which can be identified using wavenumbers at 938 and 1660 cm^{-1} (Pézolet et al., 1988). These signals are consistent with those identified in purified myosin and tropomyosin (Pascut et al., 2011; Pézolet et al., 1988). The spectral area of 1380–1490 cm^{-1} was more prominent in ventricular CMs than in atrial CMs. Pascut et al. (2011) showed that this area exhibits specific signals that can be used to discriminate CMs from non-CMs. The wavenumber region of 1380–1490 cm^{-1} refers to CH_2 and CH_3 vibrations and could signify differences in the organization of intracellular proteins (Table 1). In murine fetal development, it was demonstrated that atrial-ventricular specification is initiated before E15.5 at the fetal stage (Zammit et al., 2000). However, less is known about these developmental stages in human heart development. Notably, the Raman data we recorded from human fetal heart tissues and human cardiac cells attest a higher complexity than in the respective data from murine cells. Previously, MLC2a and MLC2v double-positive CMs were derived from hESC cultures (Mummery et al., 2012), which are also seen during normal human heart development. These CM subpopulations, which are not yet fully committed to an atrial or ventricular fate, were also noted

in our study. In future studies, Raman microspectroscopy could be further correlated to gene and protein marker expression profiles and functional measurements of these CM subpopulations. The technology could thereby help to resolve early cell fate decisions made on the path toward atrial and ventricular cardiac phenotypes (Sylva et al., 2014).

By characterizing ESC-CMs, fetal CMs, and murine adult CMs using Raman microspectroscopy, we confirmed a fetal cardiac cell phenotype profile of ESC-CMs, which is in accordance with investigations in which comparable gene expression profiles of ESC-CMs and fetal CMs were reported (Cao et al., 2008). We further showed that lipid- and protein-related Raman bands at 1266 cm^{-1}, 1437 cm^{-1}, 1658 cm^{-1} were more prominent in adult CMs than in ESC-CMs or fetal CMs. Immunofluorescence staining confirmed the presence of densely packed sarcomeric myosin in adult CMs versus more diffusely organized sarcomeric structures with shorter fragments in fetal CMs, which could be the possible reason for the spectroscopic differences that were detected in our study. Different stages of sarcomeric organization and increasing myofibril densities were also seen when employing standard methods in developing CMs (Pohjoismaki et al., 2013). In adult CMs, a lower nuclear density, higher mitochondrial density, and a metabolic shift toward β-oxidation of fatty acids was previously reported (Pohjoismaki et al., 2013). In addition, it was shown that fetal and adult CMs express differential isoforms of troponin C (Siedner et al., 2003), which might also have an impact on protein-related Raman signals at wavenumbers 1266 and 1658 cm^{-1}. Many features that are characteristic for fetal cardiac phenotypes have been described in stressed and pathological CMs (Gilsbach et al., 2014). Relapse of the MHC-isoform shift and the downregulation of fatty acid oxidation were reported as hallmarks of heart failure (Rajabi et al., 2007). Our results suggest that Raman microspectroscopy could potentially detect pathological CMs and therefore represents a very promising tool for the monitoring and diagnosis of pathological or stress-induced remodeling processes in the heart.

To summarize, in this study we demonstrated that Raman microspectroscopy can be used for the marker-free identification and characterization of different cardiac cell phenotypes and subpopulations. This technique enables the determination of the optimal endpoint in cardiac differentiation processes and facilitates a standardized characterization of in vitro-generated cardiac cells and tissues toward the goal of a clinical application.

EXPERIMENTAL PROCEDURES

Detailed information on the experimental procedures can be found in the Supplemental Information File.

Raman Microspectroscopy

All Raman spectra were recorded using a custom-built Raman microspectrometer as previously described (Brauchle et al., 2014). For all measurements, the laser power was maintained at 85 mW and the total accumulation time per spectrum was 100 s. Spectra were acquired from single living or fixed and antibody-labeled cells in suspension with medium or buffer in glass-bottom dishes (ibidi). For antibody-labeled cells, fluorescence microscopy was employed simultaneously with the Raman measurements to categorize cells according to their staining patterns. To discriminate single hESCs from their feeder layer, cells were stained for Tra-1-81 (mouse IgM conjugated to Alexa Fluor 488; Biolegend) without fixation (see Supplemental Information for details). For the identification of atrial and ventricular CMs, cells were fixed and labeled using MLC2a-FITC and MLC2v-PE (both Miltenyi Biotech; see Supplemental Information for details). FFPE tissues were de-paraffinized, rehydrated, and kept hydrated in medium or PBS buffer during the measurements. A background reference spectrum of the glass surface was taken every 5–10 spectra by measuring a cell-free and particle-free area.

Processing and Multivariate Analysis of Raman Spectra

Several mathematical processes were employed on the spectroscopic raw data to diminish background effects and to correct instrumental variations. For all spectra, background signals were subtracted, cosmic rays were removed, the spectral window was confined to the range of 400–1800 cm^{-1}, and baseline shifts were adjusted (OPUS-Software 4.2; Bruker Optics). Vector normalization was performed to assimilate all spectra in their overall signal intensity level, which are presented in arbitrary units. To increase the signal to noise ratio in the Raman spectra of histologically processed and fixed specimens, 11 data points were averaged by employing a second ordered Savitzky-Golay filtering (UnscramblerX 10.2; CAMO). PCA, which focuses on the spectral range of 400–1800 cm^{-1}, was calculated from pretreated spectra using the NIPALS algorithm (UnscramblerX 10.2). In an optimized set-up, PCA extracts valuable differences from spectral noise and random variations. In each PCA, seven principal components (PCs) were considered. All PCs were considered in the results, since even higher PCs, which cover fewer percentages of the overall variances, exhibited loading patterns with prominent biochemical signals. PC score values were further subjected to statistical analysis, which was performed using OriginPro 9.0.0G (OriginLab Corporation). PC scores were verified for normality distribution using the Kolmogorov-Smirnov test. ANOVA was employed to calculate probability values (p values) and to identify significant differences between different cell populations based on PC score values. As a model for data prediction, a discriminate analysis (LDA) was conducted based on PC scores (Chan et al., 2009). For two-dimensional scores plots, confidence ellipses, which comprised the coordinates of each spectrum in the scores plot, were calculated (95% probability).

Use of Murine and Human Tissues

The Institute of Cellular Biology and Immunology at University of Stuttgart provided adult hearts of 8-month-old female CD1 mice

and fetal mouse hearts. Appropriate surgical explantation of the murine hearts was performed in accordance with the institutional guidelines of animal ethics and care of the University of Stuttgart. Human fetal heart tissues were used in accordance with institutional guidelines and approved by the local research ethics committees at the University Hospital of the Eberhard Karls University Tuebingen (UKT) and the University of California Los Angeles (UCLA) (UKT IRB #356/2008BO2 and #406/2011BO1, UCLA IRB #05-10-093). The use of human adult heart cells was in accordance with institutional guidelines and approved by the research ethics committee of the Landesärztekammer Baden-Württemberg (IRB #F-2011-068).

SUPPLEMENTAL INFORMATION

Supplemental Information includes Supplemental Experimental Procedures, six figures, five tables, and three videos and can be found with this article online at http://dx.doi.org/10.1016/j.stemcr.2015.12.007.

AUTHOR CONTRIBUTIONS

E.B., M.G.M., S.L.L., S.B., A.N., and K.S.-L. wrote the manuscript. E.B., A.K., H.B., N.S., and S.L. conducted the experiments on cell differentiation and cell isolation and performed the Raman measurements. E.B. performed all data analysis. K.E. provided the murine hearts and performed tissue dissections. S.L.L., S.B., A.N., and K.S.-L. provided conceptual input, designed the experiments, and supervised the research.

ACKNOWLEDGMENTS

We thank Simone Pöschel (University Hospital Tübingen, ImageStream Core Facility) for her support with the imaging flow cytometry analyses. This work was financially supported by the EU Marie Curie IEF (331430 to M.G.M.); CIRM (RB3-05086 to A.N.); Fraunhofer-Gesellschaft Internal programs (Attract to K.S.-L. and FFE to S.L.L.), BMBF (0316059), Ministry of Science, Research and the Arts of Baden-Württemberg (33-729.55-3/214 and SI-BW 01222-91), and the Deutsche Forschungsgemeinschaft (INST 2388/33-1, SCHE 701/7-1, SCHE 701/10-1) (all to K.S.-L).

Received: March 8, 2015
Revised: December 4, 2015
Accepted: December 7, 2015
Published: January 14, 2016

REFERENCES

Amariglio, N., Hirshberg, A., Scheithauer, B.W., Cohen, Y., Loewenthal, R., Trakhtenbrot, L., Paz, N., Koren-Michowitz, M., Waldman, D., Leider-Trejo, L., et al. (2009). Donor-derived brain tumor following neural stem cell transplantation in an ataxia telangiectasia patient. PLoS Med. *6*, e1000029.

Bird, S.D., Doevendans, P.A., van Rooijen, M.A., Brutel de la Riviere, A., Hassink, R.J., Passier, R., and Mummery, C.L. (2003). The human adult cardiomyocyte phenotype. Cardiovasc. Res. *58*, 423–434.

Brauchle, E., Thude, S., Brucker, S.Y., and Schenke-Layland, K. (2014). Cell death stages in single apoptotic and necrotic cells monitored by Raman microspectroscopy. Sci. Rep. *4*, 4698.

Burridge, P.W., Keller, G., Gold, J.D., and Wu, J.C. (2012). Production of de novo cardiomyocytes: human pluripotent stem cell differentiation and direct reprogramming. Cell Stem Cell *10*, 16–28.

Cao, F., Wagner, R.A., Wilson, K.D., Xie, X., Fu, J.-D., Drukker, M., Lee, A., Li, R.A., Gambhir, S.S., Weissman, I.L., et al. (2008). Transcriptional and functional profiling of human embryonic stem cell-derived cardiomyocytes. PLoS One *3*, e3474.

Chan, J.W., Lieu, D.K., Huser, T., and Li, R.A. (2009). Label-free separation of human embryonic stem cells and their cardiac derivatives using Raman spectroscopy. Anal. Chem. *81*, 1324–1331.

Chung, S., Dzeja, P.P., Faustino, R.S., Perez-Terzic, C., Behfar, A., and Terzic, A. (2007). Mitochondrial oxidative metabolism is required for the cardiac differentiation of stem cells. Nat. Clin. Pract. Cardiovasc. Med., S60–S67.

Dochow, S., Beleites, C., Henkel, T., Mayer, G., Albert, J., Clement, J., Krafft, C., and Popp, J. (2013). Quartz microfluidic chip for tumour cell identification by Raman spectroscopy in combination with optical traps. Anal. Bioanal. Chem. *405*, 2743–2746.

Gilsbach, R., Preissl, S., Gruning, B.A., Schnick, T., Burger, L., Benes, V., Wurch, A., Bonisch, U., Gunther, S., Backofen, R., et al. (2014). Dynamic DNA methylation orchestrates cardiomyocyte development, maturation and disease. Nat. Commun. *5*, 5288.

Huber, I., Itzhaki, I., Caspi, O., Arbel, G., Tzukerman, M., Gepstein, A., Habib, M., Yankelson, L., Kehat, I., and Gepstein, L. (2007). Identification and selection of cardiomyocytes during human embryonic stem cell differentiation. FASEB J. *21*, 2551–2563.

Karakikes, I., Senyei, G.D., Hansen, J., Kong, C.W., Azeloglu, E.U., Stillitano, F., Lieu, D.K., Wang, J., Ren, L., Hulot, J.S., et al. (2014). Small molecule-mediated directed differentiation of human embryonic stem cells toward ventricular cardiomyocytes. Stem Cells Transl. Med. *3*, 18–31.

Kattman, S.J., Witty, A.D., Gagliardi, M., Dubois, N.C., Niapour, M., Hotta, A., Ellis, J., and Keller, G. (2011). Stage-specific optimization of activin/nodal and BMP signaling promotes cardiac differentiation of mouse and human pluripotent stem cell lines. Cell Stem Cell *8*, 228–240.

Krafft, C., Neudert, L., Simat, T., and Salzer, R. (2005). Near infrared Raman spectra of human brain lipids. Spectrochim. Acta A Mol. Biomol. Spectrosc. *61*, 1529–1535.

Leor, J., Gerecht, S., Cohen, S., Miller, L., Holbova, R., Ziskind, A., Shachar, M., Feinberg, M.S., Guetta, E., and Itskovitz-Eldor, J. (2007). Human embryonic stem cell transplantation to repair the infarcted myocardium. Heart *93*, 1278–1284.

Matsa, E., Burridge, P.W., and Wu, J.C. (2014). Human stem cells for modeling heart disease and for drug discovery. Sci. Transl. Med. *6*, 239ps236.

Mummery, C.L., Zhang, J., Ng, E.S., Elliott, D.A., Elefanty, A.G., and Kamp, T.J. (2012). Differentiation of human embryonic stem cells and induced pluripotent stem cells to cardiomyocytes: a methods overview. Circ. Res. *111*, 344–358.

Notingher, I., Bisson, I., Bishop, A.E., Randle, W.L., Polak, J.M., and Hench, L.L. (2004). In situ spectral monitoring of mRNA

translation in embryonic stem cells during differentiation in vitro. Anal. Chem. *76*, 3185–3193.

Nsair, A., Schenke-Layland, K., Van Handel, B., Evseenko, D., Kahn, M., Zhao, P., Mendelis, J., Heydarkhan, S., Awaji, O., Vottler, M., et al. (2012). Characterization and therapeutic potential of induced pluripotent stem cell-derived cardiovascular progenitor cells. PLoS One *7*, 9.

Nunes, S.S., Miklas, J.W., Liu, J., Aschar-Sobbi, R., Xiao, Y., Zhang, B., Jiang, J., Masse, S., Gagliardi, M., Hsieh, A., et al. (2013). Biowire: a platform for maturation of human pluripotent stem cell-derived cardiomyocytes. Nat. Methods *10*, 781–787.

Pascut, F.C., Goh, H.T., Welch, N., Buttery, L.D., Denning, C., and Notingher, I. (2011). Noninvasive detection and imaging of molecular markers in live cardiomyocytes derived from human embryonic stem cells. Biophys. J. *100*, 251–259.

Pasumarthi, K.B.S., and Field, L.J. (2002). Cardiomyocyte cell cycle regulation. Circ. Res. *90*, 1044–1054.

Pézolet, M., Pigeon, M., Ménard, D., and Caillé, J.P. (1988). Raman spectroscopy of cytoplasmic muscle fiber proteins. Orientational order. Biophys. J. *53*, 319–325.

Pohjoismaki, J.L.O., Kruger, M., Al-Furoukh, N., Lagerstedt, A., Karhunen, P.J., and Braun, T. (2013). Postnatal cardiomyocyte growth and mitochondrial reorganization cause multiple changes in the proteome of human cardiomyocytes. Mol. Biosyst. *9*, 1210–1219.

Puppels, G.J., de Mul, F.F., Otto, C., Greve, J., Robert-Nicoud, M., Arndt-Jovin, D.J., and Jovin, T.M. (1990). Studying single living cells and chromosomes by confocal Raman microspectroscopy. Nature *347*, 301–303.

Rajabi, M., Kassiotis, C., Razeghi, P., and Taegtmeyer, H. (2007). Return to the fetal gene program protects the stressed heart: a strong hypothesis. Heart Fail. Rev. *12*, 331–343.

Ren, L., Su, X., Wang, Y., Xu, J., and Ning, K. (2014). QSpec: online control and data analysis system for single-cell Raman spectroscopy. PeerJ *2*, e436.

Richardson, W., Wilkinson, D., Wu, L., Petrigliano, F., Dunn, B., and Evseenko, D. (2014). Ensemble multivariate analysis to improve identification of articular cartilage disease in noisy Raman spectra. J. Biophotonics *8*, 555–566.

Schenke-Layland, K., Rhodes, K.E., Angelis, E., Butylkova, Y., Heydarkhan-Hagvall, S., Gekas, C., Zhang, R., Goldhaber, J.I., Mikkola, H.K., Plath, K., et al. (2008). Reprogrammed mouse fibroblasts differentiate into cells of the cardiovascular and hematopoietic lineages. Stem Cells *26*, 1537–1546.

Siedner, S., Krüger, M., Schroeter, M., Metzler, D., Roell, W., Fleischmann, B.K., Hescheler, J., Pfitzer, G., and Stehle, R. (2003). Developmental changes in contractility and sarcomeric proteins from the early embryonic to the adult stage in the mouse heart. J. Physiol. *548*, 493–505.

Sule-Suso, J., Forsyth, N.R., Untereiner, V., and Sockalingum, G.D. (2014). Vibrational spectroscopy in stem cell characterisation: is there a niche? Trends Biotechnol. *32*, 254–262.

Sylva, M., van den Hoff, M.J., and Moorman, A.F. (2014). Development of the human heart. Am. J. Med. Genet. A *164A*, 1347–1371.

Tan, Y., Konorov, S.O., Schulze, H.G., Piret, J.M., Blades, M.W., and Turner, R.F. (2012). Comparative study using Raman microspectroscopy reveals spectral signatures of human induced pluripotent cells more closely resemble those from human embryonic stem cells than those from differentiated cells. Analyst *137*, 4509–4515.

Zammit, P.S., Kelly, R.G., Franco, D., Brown, N., Moorman, A.F., and Buckingham, M.E. (2000). Suppression of atrial myosin gene expression occurs independently in the left and right ventricles of the developing mouse heart. Dev. Dyn. *217*, 75–85.

Zwi, L., Caspi, O., Arbel, G., Huber, I., Gepstein, A., Park, I.H., and Gepstein, L. (2009). Cardiomyocyte differentiation of human induced pluripotent stem cells. Circulation *120*, 1513–1523.